Laser-Assisted Nanowelding of Graphene to Metals: An Optical Approach Toward Ultralow Contact Resistance

Article *in* Advanced Materials Interfaces · May 2017

DOI: 10.1002/admi.201700294

CITATIONS
14

READS
308

9 authors, including:

Kamran Keramatnejad
University of Nebraska at Lincoln
30 PUBLICATIONS **201** CITATIONS
SEE PROFILE

Dawei Li
Dalian University of Technology
67 PUBLICATIONS **1,071** CITATIONS
SEE PROFILE

Hossein Rabiee Golgir
32 PUBLICATIONS **470** CITATIONS
SEE PROFILE

Xi Huang
University of Nebraska at Lincoln
62 PUBLICATIONS **1,123** CITATIONS
SEE PROFILE

ADVANCED MATERIALS INTERFACES

www.advmatinterfaces.de

Laser-Assisted Nanowelding of Graphene to Metals: An Optical Approach toward Ultralow Contact Resistance

*Kamran Keramatnejad, Yun Shen Zhou, Da Wei Li, Hossein Rabiee Golgir, Xi Huang, Qi Ming Zhou, Jing Feng Song, Stephen Ducharme, and Yong Feng Lu**

The electrical performance of graphene-based devices is largely limited by substantial contact resistance at the heterodimensional graphene–metal junctions. A laser-assisted nanowelding technique is developed to reduce graphene–metal (G–M) contact resistance and improve carrier injection in suspended graphene devices. Selective breakdown of C—C bonds and formation of structural defects are realized through laser irradiation at the edges of graphene within the G–M contact regions in order to increase the chemical reactivity of graphene, facilitate G–M bonding, and, therefore, maximize interfacial carrier transportation. Through this method, significantly reduced G–M contact resistances, as low as 2.57 Ω μm are obtained. In addition, it is demonstrated that the location of laser-induced defects within the contact areas significantly impacts the interfacial properties and the carrier mobility of graphene devices. A fourfold increase in photocurrent is observed in the suspended graphene photodetectors with treated G–M interfaces as compared to ordinary ones. This contact-free and position-selective technique minimizes the degradation of the graphene channels and maintains the superior performance of graphene devices, making it a promising approach for reducing G–M resistance in the fabrication of graphene-based devices.

1. Introduction

Despite the remarkable electrical and optical properties of graphene, its successful integration into future generations of electronic devices has been bottlenecked by the presence of parasitic effects when graphene comes into contact with other materials.[1] In particular, the electrical contact resistance between graphene and metal contacts (R_C) has been reported to be a major limitation for further development of graphene electronics in emerging applications, such as photodetection,[2–4] flexible electronics,[5] transparent conducting electrodes,[6] and Hall effect sensors.[7]

K. Keramatnejad, Prof. Y. S. Zhou, Dr. D. W. Li, H. R. Golgir, X. Huang, Q. M. Zhou, Prof. Y. F. Lu
Department of Electrical and Computer Engineering
University of Nebraska–Lincoln
Lincoln, NE 68588-0511, USA
E-mail: ylu2@unl.edu

Dr. J. F. Song, Prof. S. Ducharme
Department of Physics and Astronomy
Nebraska Center for Materials and Nanoscience
University of Nebraska–Lincoln
Lincoln, NE 68588-0299, USA

DOI: 10.1002/admi.201700294

Lithography resist residue has been regarded as one of the factors that impede interfacial carrier transport at graphene–metal (G–M) interfaces. However, the reported R_C values are still far from satisfactory after cleaning via numerous methods, such as CO_2 cleaning[8] and thermal annealing,[9,10] indicating poor G–M interfaces.[9–12] Although graphene is recognized as a semimetal with zero band gap, its large density of states tends to contract at the Dirac point. Moreover, graphene behaves as an insulator for out-of-plane carrier transport due to the difference between its Dirac-type carriers and the Schrodinger-type carriers in metals, which also leads to an increased R_C.[11,13] In some metals, such as Au, this limitation is further intensified due to the weak van der Waals (vdW) force between the metal and the chemically inert graphene leading to an additional tunnel barrier for carrier transport.[11] Therefore, formation of strong chemical bonding at the G–M interface with a short coupling length is crucial for improving the interfacial carrier transmission in graphene devices.[11,14]

Theoretical studies have demonstrated that G–M bonding occurs only at positions where dissociated C—C bonds and open edges of graphene are present. Numerous methods, such as ultraviolet (UV) ozone treatment,[15] low-power O_2 plasma etching,[16] and patterning of the graphene[17,18] have been proposed to improve the chemical activity of graphene by introducing structural defects. However, the randomly formed defects and extra lithographic processing steps could lead to unwanted amorphization, contamination, and degradation of the graphene. It is, therefore, essential that new techniques be developed to overcome the challenges existing in current methods of G–M bonding.

Based on the versatile laser–material interactions, laser-enabled techniques for facilitating micro/nanofabrication, such as structural patterning,[19] solid-phase doping,[20] material growth,[21] and chemical functionalization,[22] have been extensively investigated. Specifically, laser-induced structural modifications in graphene have been reported to be effective for alteration of its properties such as doping,[20] defect density,[23] and hydrophobic properties.[24] In our previous studies, implementation of carbon nanotubes (CNTs) as low-resistance electrical channels onto Cu substrates was

achieved by laser irradiation with significantly reduced CNT–Cu resistance.[25]

Here we report the development of a laser-assisted nanowelding technique that significantly reduces G–M contact resistance (R_C) without degrading graphene channels and compromising device performance. Structural defects are generated at the edges of graphene through localized laser-induced breakdown of C—C bonds in order to increase the chemical reactivity of graphene within the contact area while keeping its main structure intact. Au, interacting weakly with graphene,[26] was chosen as the metal contact. Mechanically exfoliated graphene was directly transferred onto metal contacts and suspended from the SiO_2 substrates in order to minimize effects, such as charge trapping and surface charging, that could interfere with the study of the contact resistance.[2,27,28] This method was performed at different positions of graphene within the contact areas in order to study the impacts of the irradiation location on the R_C values and carrier mobility of graphene. Finally, the laser-assisted nanowelding method was used to improve the photoresponsive performance in photodetectors containing suspended graphene channels.

2. Results and Discussion

The laser-irradiation step, as depicted in **Figure 1**a, was carried out using a continuous-wave (CW) laser with a wavelength of 514 nm, which is below the reported ablation threshold for graphene[29] and is in the spectral range where the Au thin film is highly reflective and optically nonabsorbent, in order to avoid damage to the electrodes.[30] The fluence was set at 6.24×10^9 J cm^{-2}, which is higher than the threshold value for the sp^2 C—C bond breaking.[31] Since the photon energy of the laser is lower than the binding energy of graphene, the disassembly of these bonds occurs mainly due to the recombination of the photogenerated electron–hole pairs during intense illumination of graphene.[31,32] Bonds between the open-ended C atoms and metal atoms are then feasible through a thermal annealing step.[10,18] Mechanically exfoliated few-layer graphene with similar number of layers (thickness ≈ 5 nm; Figure S2, Supporting Information) was used to fabricate four-point probe devices with various contact areas (A_C) (see the Experimental Section for details). Figure 1b shows a scanning electron microscope (SEM) image of a typical four-point probe device fabricated for this study. The graphene channel was studied before each step of the experiment using atomic force microscopy (AFM), as depicted in Figure 1c. As observed, the height of the graphene (white dashed line in the AFM image) was around 27 nm, confirming the suspended structure of graphene. Note that all of the prepared devices discussed in this work were annealed in a forming gas environment (10 torr, 5% H_2–95% Ar) at 400 °C for 1 h prior to the laser irradiation experiment in order to remove contaminants, such as the polymer gel used for graphene transfer.

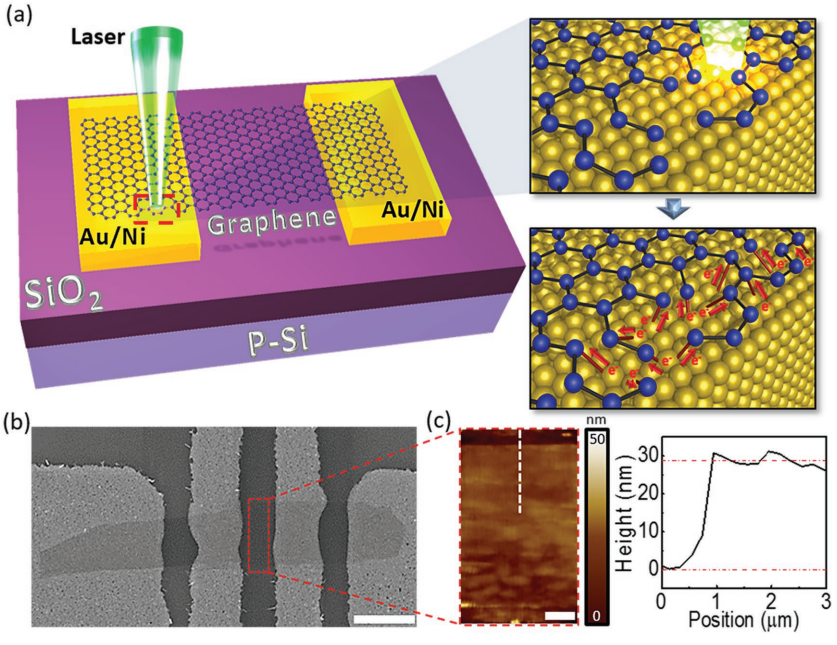

Figure 1. a) Schematic representation of the laser-assisted nanowelding process on a suspended graphene device based on the formation of laser-induced structural defects and open-ended C-atoms and subsequent realization of strong G–M bonding at the laser-irradiated areas after the thermal treatment. b) SEM micrograph of a typical four-point probe structure consisting of suspended graphene (scale bar = 5 μm). c) AFM image of the suspended graphene channel in the red rectangle in (b), along with the corresponding thickness profile obtained along the width of the channel (white dashed line in the AFM image, scale bar = 1 μm).

2.1. Laser-Assisted Nanowelding at the Edges of Graphene

The edges of the graphene at the G–M interfaces were irradiated, as shown in **Figure 2**a. The value of R_C was calculated via Equation (1)

$$R_C = \frac{1}{2}(R_{2P} + R_{Ch}) \times W \quad (1)$$

where R_{2p} is the two-point resistance, R_{Ch} is the channel resistance obtained from four-point measurement, and W is the width of the graphene channel (see Figure 2a). Figure 2b displays the average value of R_C for samples of various A_C after every step. The pristine R_C increased proportional to the value of A_C due to the vdW barriers between Au and graphene.[33,34] All samples exhibited an increase in R_C after the laser-irradiation step, which was related to the laser-induced formation of defects at the edges. This variation, however, did not exceed 10% of the pristine R_C value, since only a small portion of the contact area was irradiated. A reduction in R_C was measured after the laser-processed samples were thermally annealed at T = 400 °C for 1 h. It is notable that the improvements observed were far more substantial for the laser-irradiated devices, compared to the

ones reported after a single annealing step in other studies.[35] In particular, R_C at A_C = 3.3 μm^2 was reduced to 2.57 Ω μm, less than 16% of its pristine value after the annealing step. This value is also close to the projected values for a 22 nm channel length.[11] The ratio of the processed contact resistance to its pristine value $\left(\frac{R_{C-New}}{R_{C-Pristine}}\right)$ after each step was calculated and the results are shown in Figure 2c. This ratio was reduced from 2.13 to 1.08 after the laser-irradiation step as A_C increased. This observation further supports the suggestion that the pristine side-contact resistance is mostly dependent on the weak vdW bonding formed between graphene and Au.[33] Since only the edges of the graphene were irradiated, less severe changes were expected as the A_C increased. The $\frac{R_{C-New}}{R_{C-Pristine}}$ values after the annealing step were consistently less than 1 and in reverse relation with A_C, indicating an overall reduction in R_C and more significant improvement as the devices were scaled down.

Figure 2d shows the Raman spectra taken at the graphene edges (P1 in Figure 2a) compared to the one obtained from the central area (P2 in Figure 2a) after each step. As noted, the pristine graphene flake exhibited uniform spectra without a notable D-band at both positions, which is to be expected of graphene with a perfect lattice structure and weak bonding with the Au electrode.[10] After the laser-irradiation step, a D-band of around 1350 cm^{-1} was observed at P1 due to the structural disruption at the edge of the graphene caused by laser irradiation. The D-band emission was still observed after the thermal annealing step at P1, while at P2, the Raman spectra remained unchanged throughout the whole treatment. These observations were consistent throughout the total contact area. Mapping the D/G ratio, the square red-lined area in Figure 2a, and comparing Figure 2e and Figure 2f reveals a monotonic rise in the D/G ratio at the graphene edges after the laser irradiation. In addition, it can be noted that this parameter remained unaffected and stayed at its lowest value at the graphene channel area. In other words, no structural disruption occurred at the channel throughout the steps, reflecting the selective mechanism of the laser-assisted nanowelding method, where structural modifications were localized at the edges of the contact areas, while the graphene channels remained unaffected.

Based on the results from the electrical measurements and Raman spectra obtained after each step of the laser-assisted nanowelding process, it was evident that carrier transportation across the G–M interfaces was significantly enhanced through the formation of additional carrier transport channels at the treated G–M interfaces. According to recent first-principles nonequilibrium Green's function studies reported by Ma et al., carrier injection between graphene and weakly interacting metals, such as Au, can be significantly increased if open graphene edges and point defects are present at the G–M interface.[33] The qualitative agreement between this proposed mechanism and the improvements observed in our studies suggests that laser irradiation leads to the disturbance in the structure of graphene and the generation of chemically active and open-ended dangling bonds (see Figure 2d–f), which subsequently

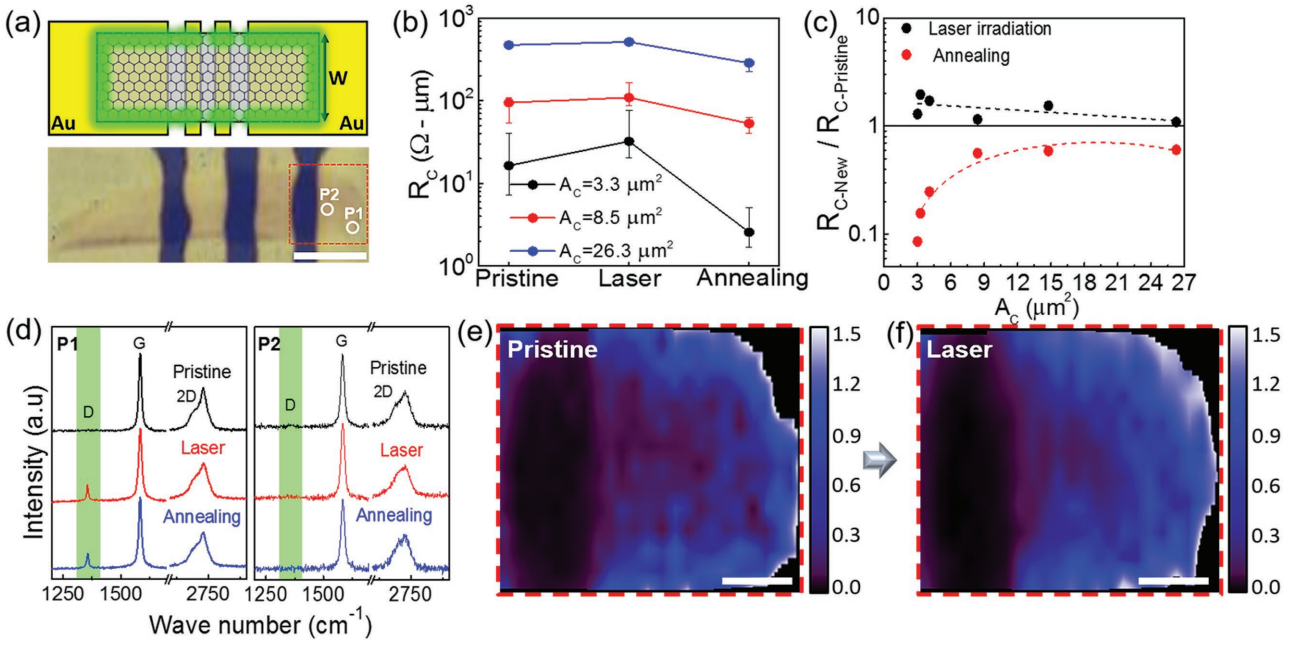

Figure 2. a) Top: schematics of the laser-irradiation step at the edges of graphene, indicated with green lines. Bottom: the optical image taken from a typical four-point probe suspended graphene device (scale bar = 5 μm). b) The calculated R_C values along with their experimental uncertainties (Figure S3, Supporting Information) obtained after each step of the laser-assisted nanowelding process for various device sizes. c) The calculated $\frac{R_{C-New}}{R_{C-Pristine}}$ ratio after each step of the process. d) A comparison between the Raman spectrums taken at the edge of graphene where the laser-irradiation step was performed (P1 in the optical image of (a)) and the center of graphene (P2 in the optical image of (a)). Raman maps in (e) and (f) illustrate the D/G ratio of the area indicated in the red dashed rectangle in the optical image of (a), prior to the treatment and after the laser irradiation of the edges, respectively (scale bar = 1 μm).

form a strong coupling with metal atoms after the annealing step at the laser-irradiated spots. Furthermore, it is critical to note that the improvements observed herein are far more drastic compared to the ones reported for single-annealing methods on physisorbed metals, such as Au,[9,10] further supporting the above interpretation.

We also investigated the effect of annealing duration on R_C for a number of devices by extending the annealing time and found that improvements were negligible for durations longer than 1 h (Figure S4, Supporting Information).

In addition, the localized irradiation of the graphene at its edges created defective areas that were small, with respect to the graphene sheet; and this prevented a comprehensive structural degradation and shrinkage of its effective width, which can cause scattering, band gap widening, and increased R_C.[36]

2.2. Laser-Assisted Nanowelding at the Center of Graphene

We studied the effect of laser irradiation performed at the center of the contact area, as schematically shown in **Figure 3**a. All of the parameters chosen for the laser irradiation and its following annealing step were the same as those described in the previous section, except that the center area of the G–M interface was irradiated instead of the edges. The electrical characterizations shown in Figure 3b illustrate an increase in R_C for all of the samples after the laser-irradiation step, similar to what was observed in Figure 2b; and R_C was increased for the samples with $A_C > 3\ \mu m^2$, after the annealing step. The calculated $\frac{R_{C-New}}{R_{C-Pristine}}$ ratio plotted in Figure 3c shows a slight increase with respect to A_C after the laser-irradiation step. Since the majority of the interface was irradiated, more severe changes were expected due to the formation of massive defects when compared to Figure 2c. Interestingly, the resulting ratios after the annealing step became larger than 1 for $A_C > 5\ \mu m^2$, which is in contrast to what was observed in Figure 2c. The reasons behind the contradictory outcomes of the laser-assisted nanowelding method performed at different parts of the G–M interface can be justified by studying the impact of this treatment method on the carrier mobility (μ) of graphene. This parameter has been proven to have different values at the suspended parts of graphene versus the areas supported by the electrodes.[2,7,26,27] Since the location-selective mechanism in our proposed method excludes potential impacts on the channel, it is reasonable to suggest that the major effects on the mobility came from the G–M interface. The mobility of the devices was extracted via Equation (2)

$$\mu = \frac{1}{ne\rho_{\square}} \tag{2}$$

where $\rho_{\square}$ is the sheet resistance obtained from four-point measurements, n is the carrier density of graphene, and e is the electron charge. n was extracted by matching the channel

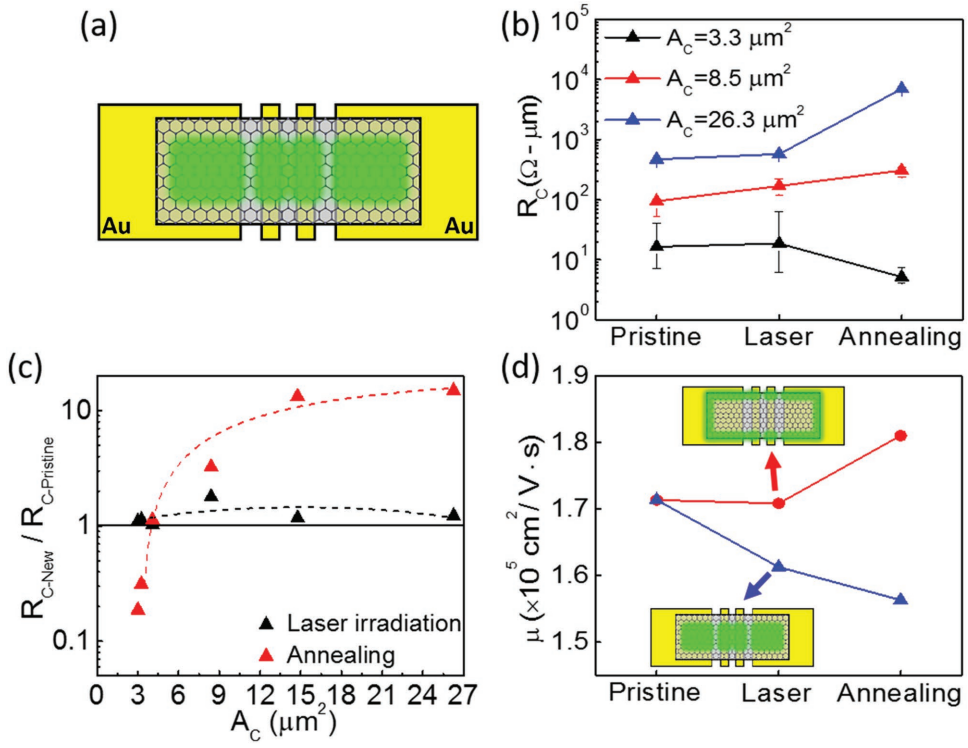

Figure 3. a) Schematics of the device during the laser-irradiation step performed at the center of the graphene, indicated with the green area. b) Average R_C values along with their experimental uncertainties obtained after each step of the process for various device sizes. c) The calculated $\frac{R_{C-New}}{R_{C-Pristine}}$ ratio after each step of the process performed at the center of graphene. d) The calculated mobility at each step of the two laser-assisted nanowelding processes performed at various locations of graphene. Note: the insets illustrate the laser-irradiated areas for each dataset.

conductivities obtained with Hall measurements reported on similar suspended structures.[7,37] The calculated mobilities of the devices studied are shown in Figure 3d ranging between 150 000 and 190 000 $cm^2\ V^{-1}\ s^{-1}$ and are close to previously reported values for suspended graphene structures.[7,27,30,37,38] It can be noted that mobility decreased for both cases after the laser-irradiation step, which is in accordance with the observations in Figures 2b and 3b. The slope of this reduction is slightly larger for the case of irradiation at the central area, which can be related to the fact that a larger portion of the contact area is irradiated, compared to case of edge-irradiation. Interestingly, it was further observed in Figure 3d that the mobility of the edge-irradiated samples increased after the annealing step, whereas it dropped significantly for the center-irradiated samples. This implies that the structural disruption and, accordingly, the bonding formation at the edges of the graphene improves the carrier injection efficiency. In addition, it preserves the electronic structure and, therefore, superior carrier mobility at its main part. For laser irradiation at the central areas, however, formation of these structural defects would be at the cost of degraded in-plane mobility, as observed in Figure 3d (blue data points). The selective mechanism of our approach gives the advantage of forming edge-contacts at the G–M interface with minimal effect on the mobility of graphene.

3. Laser-Assisted Nanowelding of Suspended Graphene Photodetectors

Photodetectors, consisting of suspended graphene channels, were fabricated and processed using the laser-assisted nanowelding method. As shown in the optical image in **Figure 4**a, a suspended graphene device on Au electrodes was prepared via a similar fabrication method, as previously discussed. The steps were performed using similar parameters as discussed above. Corresponding electrical properties complied with the same trends, as depicted in Figure 2b,c (Figure S5, Supporting Information).

The photoresponse of the device was characterized by scanning photocurrent microscopy measurements.[39,40] As shown in Figure 4a, the photocurrent of the device under V_{DS} = 0.0 V bias was recorded while scanning a focused laser beam with spot size of 1 µm along the length of the graphene sheet. The photocurrent measurement result of the device before and after the laser-assisted nanowelding is shown in Figure 4b. The photocurrent of the pristine device reached its maximum at the suspended area, which was consistent with the previous reports[3] and can be attributed to the absence of electron energy decay channels and extrinsic disorder that originated from the substrate.[2,27,41] However, this parameter almost quadrupled after laser-assisted nanowelding; and the response contrast between the contact areas and the suspended channel became more significant. This improvement can be attributed to the intensification of the photoelectric effect in the treated device. Improving the interfacial carrier transport after the laser-assisted nanowelding process reduced the chances of scattering or recombination of the photoexcited carriers that occur mostly at the contacts, due to the weak G–M coupling and strong contact barrier.[3,27,42] In addition, the photoelectric mechanism leads to a faster optical response time, compared to the thermoelectric effect that is reported to be mainly responsible in weakly coupled junctions.[3,43] Therefore, the fourfold amplification of the photocurrent obtained through our laser-assisted nanowelding method creates an opportunity for fabrication of highly responsive photodetectors.

4. Conclusion

In conclusion, we have developed a laser-assisted nanowelding technique to reduce G–M contact resistance by realizing an edge-contacted configuration between graphene and Au. Localized laser irradiation was performed to generate unsaturated C atoms and chemically active point defects at the edges of graphene and to facilitate the G–M bonding after the subsequent thermal annealing step. This structural modification at the interfaces, which was verified through Raman spectroscopy, resulted in R_C values as low as 2.57 Ω µm. The improvements in electrical performance of the suspended graphene devices were intensified as the devices were scaled down, which indicates the potential for the laser-assisted nanowelding method to be integrated into future process flows for graphene devices. We further demonstrated that the advantage of this technique is precise structural modifications, without reducing the high in-plane carrier mobility of the graphene channel. Based on the technique developed, a fourfold increase in the photocurrent was achieved in the suspended-graphene devices, further demonstrating the potential of this approach for improving the performance of graphene-based optical devices.

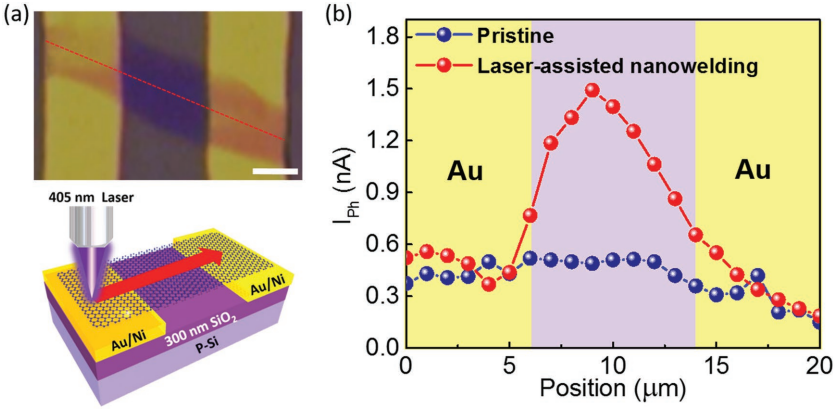

Figure 4. a) Optical image taken from the suspended graphene device prepared for the photocurrent mapping along with the schematics of this experiment. The red dashed line shows the scanning direction of the 405 nm laser (scale bar = 1 µm). b) The photocurrent mapping results obtained for the device before and after the laser-assisted nanowelding process. A fourfold increase in the photocurrent was obtained at the suspended area after the laser-assisted nanowelding process.

5. Experimental Section

Mechanical Exfoliation of Graphene: Graphene flakes were prepared by mechanically exfoliating commercial highly ordered pyrolytic graphite, (MikroMasch/ZYH/DS/1) using Scotch transparent tape.

Fabrication of Suspended Graphene–Au Structures: A standard photolithography/lift-off procedure was utilized to pattern the Ni/Au (5/30 nm) contacts on SiO_2 (300 nm)/Si substrate by sputtering. The dry transfer technique was then used for mounting the graphene flake on top of metal contacts.[44] The detailed steps of this method are described in Figure S1 (Supporting Information). Finally, a 400 °C annealing step under the forming gas environment (5%H_2–95%Ar) was applied on the devices for 1 h at a total pressure of 10 torr, in order to burn off possible impurities and polymer contaminants.

Laser Irradiation of the G–M Interface: For the laser-irradiation step, the devices were irradiated in air at room temperature using a CW argon ion laser ($\lambda = 514$ nm, average power = 20 mW, fluence = 6.24×10^9 J cm^{-2}, spot size = 700 nm; Modu-Laser, Stellar-RMN 514/50), which was integrated into a confocal Raman microscope with a ×100 objective. The laser scanning step size was kept at 500 nm, which is smaller than the laser spot size, in order to realize the comprehensive irradiation. The scanning speed was programmed to be 5 Å s^{-1} with moving fashions of single-axis and parallel scanning for the cases of edge-irradiation (Figure 2a) and center-irradiation (Figure 3a), respectively.

Thermal Annealing: All of the annealing processes in this study were performed using a tube furnace (RTP4-080811P, 4 inch, MRI Corp) at a total pressure of 1–5 mtorr, unless otherwise specified.

Electrical Characterization: All electrical characterizations were conducted using an Agilent 4155C semiconductor parameter analyzer connected to a probe station (Cascade Microtech, MPS150) equipped with High-Voltage Parameteric (HVP) probes.

Raman Spectroscopy: Raman spectroscopic studies were performed using a micro-Raman spectrometer (Renishaw InVia plus, Renishaw) at room temperature. An argon ion laser ($\lambda = 514$ nm) with an output power of 3.0 mW was used as the excitation source, and the spectra was collected using a ×50 objective lens with an accumulation of 1.0 s per position.

Atomic Force Microscopy: The morphological studies were performed using an AFM (afm+, Anasys Instruments) in the tapping mode.

Scanning Photocurrent Microscopy: The sample was illuminated by a 1 mW blue diode laser beam ($\lambda = 405$ nm, fluence = 1.6×10^3 J cm^{-2}) modulated by a chopper at 40 Hz to reduce the thermal effect of the laser on the sample. The laser beam was tightly focused into a 1 μm spot size to enhance the spatial resolution.[45] The photocurrent was collected with an SR830 lock-in amplifier at each scanning step with the chopper frequency as a reference.

Supporting Information

Supporting Information is available from the Wiley Online Library or from the author.

Acknowledgements

This research work was financially supported by the National Science Foundation (CMMI 1265122), the Nebraska Materials Research Science and Engineering Center (MRSEC, DMR-1420645), and the Nebraska Center for Energy Sciences Research (NCESR).

Conflict of Interest

The authors declare no conflict of interest.

Keywords

contact resistance, edge contact, graphene-metal interfaces, laser irradiation, suspended graphene

Received: March 9, 2017
Revised: April 9, 2017
Published online:

[1] a) G. Fiori, F. Bonaccorso, G. Iannaccone, T. Palacios, D. Neumaier, A. Seabaugh, S. K. Banerjee, L. Colombo, *Nat. Nanotechnol.* **2014**, *9*, 768; b) International Technology Roadmap for Semiconductors 2012, Semiconductor Industry Association, http://www.itrs.net/Links/2012ITRS/Home2012.htm (accessed: March 2017); c) K. S. Novoselov, V. Fal, L. Colombo, P. Gellert, M. Schwab, K. Kim, *Nature* **2012**, *490*, 192; d) F. Xia, V. Perebeinos, Y.-M. Lin, Y. Wu, P. Avouris, *Nat. Nanotechnol.* **2011**, *6*, 179.
[2] M. Freitag, T. Low, P. Avouris, *Nano Lett.* **2013**, *13*, 1644.
[3] V. Patil, A. Capone, S. Strauf, E.-H. Yang, *Sci. Rep.* **2013**, *3*, 2791.
[4] G. Rao, M. Freitag, H.-Y. Chiu, R. S. Sundaram, P. Avouris, *ACS Nano* **2011**, *5*, 5848.
[5] L. Gomez De Arco, Y. Zhang, C. W. Schlenker, K. Ryu, M. E. Thompson, C. Zhou, *ACS Nano* **2010**, *4*, 2865.
[6] a) H. Park, P. R. Brown, V. Bulović, J. Kong, *Nano Lett.* **2011**, *12*, 133; b) X. Wang, L. Zhi, K. Müllen, *Nano Lett.* **2008**, *8*, 323.
[7] K. I. Bolotin, F. Ghahari, M. D. Shulman, H. L. Stormer, P. Kim, *Nature* **2009**, *462*, 196.
[8] S. Gahng, C. H. Ra, Y. J. Cho, J. A. Kim, T. Kim, W. J. Yoo, *Appl. Phys. Lett.* **2014**, *104*, 223110.
[9] W. S. Leong, H. Gong, J. T. Thong, *ACS Nano* **2013**, *8*, 994.
[10] W. S. Leong, C. T. Nai, J. T. Thong, *Nano Lett.* **2014**, *14*, 3840.
[11] A. Allain, J. Kang, K. Banerjee, A. Kis, *Nat. Mater.* **2015**, *14*, 1195.
[12] K. Nagashio, T. Nishimura, K. Kita, A. Toriumi, presented at *Electron Devices Meeting (IEDM), 2009 IEEE International*, MD, USA, December **2009**.
[13] R. Ifuku, K. Nagashio, T. Nishimura, A. Toriumi, *Appl. Phys. Lett.* **2013**, *103*, 033514.
[14] a) C. Gong, S. McDonnell, X. Qin, A. Azcatl, H. Dong, Y. J. Chabal, K. Cho, R. M. Wallace, *ACS Nano* **2013**, *8*, 642; b) Y. Khatami, H. Li, C. Xu, K. Banerjee, Electron Devices, *IEEE Trans. Electron Devices* **2012**, *59*, 2444; c) P. Pomorski, C. Roland, H. Guo, *Phys. Rev. B* **2004**, *70*, 115408; d) P. Tarakeshwar, D. M. Kim, *J. Phys. Chem. B* **2005**, *109*, 7601.
[15] a) C. W. Chen, F. Ren, G.-C. Chi, S.-C. Hung, Y. Huang, J. Kim, I. I. Kravchenko, S. J. Pearton, *J. Vac. Sci. Technol., B: Nanotechnol. Microelectron.: Mater., Process., Meas., Phenom.* **2012**, *30*, 060604; b) W. Li, Y. Liang, D. Yu, L. Peng, K. P. Pernstich, T. Shen, A. H. Walker, G. Cheng, C. A. Hacker, C. A. Richter, *Appl. Phys. Lett.* **2013**, *102*, 183110.
[16] J. A. Robinson, M. LaBella, M. Zhu, M. Hollander, R. Kasarda, Z. Hughes, K. Trumbull, R. Cavalero, D. Snyder, *Appl. Phys. Lett.* **2011**, *98*, 053103.
[17] H. Y. Park, W. S. Jung, D. H. Kang, J. Jeon, G. Yoo, Y. Park, J. Lee, Y. H. Jang, J. Lee, S. Park, *Adv. Mater.* **2015**, *28*, 864.
[18] J. T. Smith, A. D. Franklin, D. B. Farmer, C. D. Dimitrakopoulos, *ACS Nano* **2013**, *7*, 3661.
[19] a) J. Park, W. Xiong, Y. Gao, M. Qian, Z. Xie, M. Mitchell, Y. Zhou, G. Han, L. Jiang, Y. Lu, *Appl. Phys. Lett.* **2011**, *98*, 123109; b) R. S. Singh, V. Nalla, W. Chen, A. T. S. Wee, W. Ji, *ACS Nano* **2011**, *5*, 5969.
[20] I. Choi, H. Y. Jeong, D. Y. Jung, M. Byun, C.-G. Choi, B. H. Hong, S.-Y. Choi, K. J. Lee, *ACS Nano* **2014**, *8*, 7671.

[21] a) H. R. Golgir, Y. Gao, Y. Zhou, L. Fan, K. Keramatnejad, Y. Lu, presented at *Proc. 33rd International Congress on Applications of Lasers and Electro-Optics (ICALEO)*, October **2014**, Atlanta, GA, USA; b) H. R. Golgir, Y. S. Zhou, D. Li, K. Keramatnejad, W. Xiong, M. Wang, L. J. Jiang, X. Huang, L. Jiang, J. F. Silvain, *J. Appl. Phys.* **2016**, *120*, 105303; c) Y. Lu, H. R. Golgir, Y. Zhou, U.S. Patent Application No. 15/158,305, **2016**; d) H. Rabiee Golgir, Y. Gao, Y. S. Zhou, L. Fan, P. Thirugnanam, K. Keramatnejad, L. Jiang, J.-F. O. Silvain, Y. F. Lu, *Cryst. Growth Des.* **2014**, *14*, 6248.
[22] a) W. H. Lee, J. W. Suk, H. Chou, J. Lee, Y. Hao, Y. Wu, R. Piner, D. Akinwande, K. S. Kim, R. S. Ruoff, *Nano Lett.* **2012**, *12*, 2374; b) A. F. Zedan, S. Moussa, J. Terner, G. Atkinson, M. S. El-Shall, *ACS Nano* **2012**, *7*, 627.
[23] S. Pei, H.-M. Cheng, *Carbon* **2012**, *50*, 3210.
[24] H. B. Jiang, Y. L. Zhang, D. D. Han, H. Xia, J. Feng, Q. D. Chen, Z. R. Hong, H. B. Sun, *Adv. Funct. Mater.* **2014**, *24*, 4595.
[25] K. Keramatnejad, Y. S. Zhou, Y. Gao, H. R. Golgir, M. Wang, L. Jiang, J.-F. Silvain, Y. F. Lu, *J. Appl. Phys.* **2015**, *118*, 154311.
[26] Q. M. Ramasse, R. Zan, U. Bangert, D. W. Boukhvalov, Y.-W. Son, K. S. Novoselov, *ACS Nano* **2012**, *6*, 4063.
[27] D.-K. Ki, A. F. Morpurgo, *Nano Lett.* **2013**, *13*, 5165.
[28] H. Momtazbaf, Effect of Geometry and Gate Voltage on the Conductance of an Ideal Strip of Graphene, Masters thesis, University of Victoria, **2015**.
[29] H. O. Jeschke, M. E. Garcia, K. Bennemann, *Phys. Rev. Lett.* **2001**, *87*, 015003.
[30] M. Bass, C. DeCusatis, J. Enoch, V. Lakshminarayanan, G. Li, C. Macdonald, V. Mahajan, E. Van Stryland, *Handbook of Optics, Volume II: Design, Fabrication and Testing, Sources and Detectors, Radiometry and Photometry*, McGraw-Hill, New York, USA, **2009**.
[31] G. Amato, G. Milano, U. Vignolo, E. Vittone, *Nano Res.* **2015**, *8*, 3972.
[32] B. Krauss, T. Lohmann, D.-H. Chae, M. Haluska, K. von Klitzing, J. H. Smet, *Phys. Rev. B* **2009**, *79*, 165428.
[33] B. Ma, C. Gong, Y. Wen, R. Chen, K. Cho, B. Shan, *J. Appl. Phys.* **2014**, *115*, 183708.
[34] R. S. Sundaram, M. Steiner, H.-Y. Chiu, M. Engel, A. A. Bol, R. Krupke, M. Burghard, K. Kern, P. Avouris, *Nano Lett.* **2011**, *11*, 3833.
[35] A. Babichev, V. Gasumyants, A. Y. Egorov, S. Vitusevich, M. Tchernycheva, *Nanotechnology* **2014**, *25*, 335707.
[36] M. Y. Han, B. Özyilmaz, Y. Zhang, P. Kim, *Phys. Rev. Lett.* **2007**, *98*, 206805.
[37] A. Laitinen, M. Oksanen, A. Fay, D. Cox, M. Tomi, P. Virtanen, P. J. Hakonen, *Nano Lett.* **2014**, *14*, 3009.
[38] D. Wang, X. Liu, L. He, Y. Yin, D. Wu, J. Shi, *Nano Lett.* **2010**, *10*, 4989.
[39] a) Q. Dong, J. Song, Y. Fang, Y. Shao, S. Ducharme, J. Huang, *Adv. Mater.* **2016**; b) D. Li, W. Xiong, L. Jiang, Z. Xiao, H. Rabiee Golgir, M. Wang, X. Huang, Y. Zhou, Z. Lin, J. Song, *ACS Nano* **2016**, *10*, 3766.
[40] D. W. Li, Z. Xiao, H. R. Golgir, L. J. Jiang, V. R. Singh, K. Keramatnejad, K. E. Smith, X. Hong, L. Jiang, J. F. Silvain, *Adv. Electronic Mater.* **2017**, *3*, 1600335.
[41] T. Low, V. Perebeinos, R. Kim, M. Freitag, P. Avouris, *Phys. Rev. B* **2012**, *86*, 045413.
[42] a) E. V. Castro, H. Ochoa, M. Katsnelson, R. Gorbachev, D. Elias, K. Novoselov, A. Geim, F. Guinea, *Phys. Rev. Lett.* **2010**, *105*, 266601; b) X. Du, I. Skachko, A. Barker, E. Y. Andrei, *Nat. Nanotechnol.* **2008**, *3*, 491.
[43] K. Keramatnejad, F. Khorramshahi, S. Khatami, E. Asl-Soleimani, *Optical and Quantum Electronics.* **2015**, *47*, 1739.
[44] A. Castellanos-Gomez, M. Buscema, R. Molenaar, V. Singh, L. Janssen, H. S. van der Zant, G. A. Steele, *2D Mater.* **2014**, *1*, 011002.
[45] J. Song, H. Lu, A. Gruverman, S. Ducharme, *Appl. Phys. Lett.* **2014**, *104*, 192901.

